JACS
JOURNAL OF THE AMERICAN CHEMICAL SOCIETY

Article

Multi-step Engineering of Synergistic Catalysts in a Metal-Organic Framework for Tandem C-O Bond Cleavage

Yang Song, Xuanyu Feng, Justin S Chen, Carter Brzezinski, Ziwan Xu, and Wenbin Lin

J. Am. Chem. Soc., **Just Accepted Manuscript** • DOI: 10.1021/jacs.0c00073 • Publication Date (Web): 20 Feb 2020

is published by the American Chemical Society. 1155 Sixteenth Street N.W., Washington, DC 20036

Multi-step Engineering of Synergistic Catalysts in a Metal-Organic Framework for Tandem C-O Bond Cleavage

Yang Song,† Xuanyu Feng,† Justin S. Chen, Carter Brzezinski, Ziwan Xu, and Wenbin Lin*

Department of Chemistry, The University of Chicago, 929 East 57th Street, Chicago, IL 60637, USA

ABSTRACT: Cleavage of strong C-O bonds without breaking C-C/C-H bonds is a key step for catalytic conversion of renewable biomass to hydrocarbon feedstocks. Herein we report multi-step sequential engineering of orthogonal Lewis acid and palladium nanoparticle (NP) catalysts in a metal-organic framework (MOF) built from $(Al\text{-}OH)_n$ secondary building units and a mixture of 2,2'-bipyridine-5,5'-dicarboxylate(dcbpy) and 1,4-benzenediacrylate (pdac) ligands (**1**) for tandem C-O bond cleavage. Ozonolysis of **1** selectively removed pdac ligands to generate $Al_2(OH)(OH_2)$ sites which were subsequently triflated with trimethyl triflate (Me_3SiOTf) to afford strongly Lewis acidic sites for dehydroalkoxylation. Coordination of $Pd(MeCN)_2Cl_2$ to dcbpy ligands followed by *in situ* reduction produced orthogonal Pd NP sites in **1**-OTf-Pd^{NP} as the hydrogenation catalyst. Selective and precise transformation of **1** into **1**-OTf-Pd^{NP} was characterized step-by-step using powder X-ray diffraction, transmission electron microscopy, thermogravimetric analysis, inductively coupled plasma-mass spectrometry, infrared spectroscopy, and X-ray absorption spectroscopy. Hierarchical incorporation of orthogonal Lewis acid and Pd NP active sites endowed **1**-OTf-Pd^{NP} outstanding catalytic performance in apparent hydrogenolysis of etheric, alcoholic, and esteric C-O bonds to generate saturated alkanes via a tandem dehydroalkoxylation-hydrogenation process under relatively mild conditions. The reactivity of C-O bonds followed the trend of tertiary carbon > secondary carbon > primary carbon. Control experiments demonstrated the heterogeneous nature and recyclability of **1**-OTf-Pd^{NP} and its superior catalytic activity over the homogeneous counterparts. Sequential engineering of multiple catalytic sites in MOFs thus present a unique opportunity to address outstanding challenges in sustainable catalysis.

INTRODUCTION

The conversion of abundant and renewable biomass into value-added hydrocarbon feedstocks provides a potential sustainable solution to an ever-increasing global need for commodity chemicals and fuels.[1-3] The key step of biomass conversion involves reducing the oxygen content (~40%) without breaking C-C/C-H bonds.[4-8] In the presence of hydrogen, strong C-O bonds of alcohols, ethers, and esters in abundant lignocellulosic biomass can be selectively cleaved in a hydrodeoxygenation process.[9-13] Development of novel catalytic technologies for efficient hydrodeoxygenation of C-O bonds in biomass offers a viable pathway towards green, efficient, and economic biomass utilization and establishing the bio-renewable industry.[14]

Among many strategies for the catalytic hydrodeoxygenation of lignocellulosic biomass,[15-25] one-pot tandem catalysis offers an efficient method to break strong C-O bonds and transform biomass into valuable hydrocarbon fuels.[26-29] In particular, Marks and coworkers coupled tandem catalytic cycles of C-O dehydroalkoxylation and olefin hydrogenation to drive hydrogenolysis of ethers, alcohols, and esters with a combination of homogeneous Lewis acid catalysts and Pd nanoparticles (NPs).[30-34] Thermodynamic analysis revealed that exothermic Pd NP-catalyzed hydrogenation cycle could compensate endothermic acid-catalyzed C-O dehydroalkoxylation cycle to render the overall reaction exothermic.[30, 35] However, the effectiveness of this tandem catalytic hydrodeoxygenation process is limited by the reliance on non-reusable homogenous Lewis acid catalysts $M(OTf)_n$ (M =Hf, Al, Zr, etc) and the deactivation of metallic Pd NPs at elevated reaction temperatures. The propensity for interference between homogeneous Lewis acidic $M(OTf)_n$ sites and Pd NPs adds another challenge to achieving long-term catalytic activities with truly orthogonal active sites, which is a common problem for other multi-catalytic systems involving homogeneous catalysts.[36-38]

Metal-organic frameworks (MOFs) have emerged as a versatile and tunable porous material platform for the design of structurally and functionally uniform solid catalysts over the past two decades.[39-43] As catalytic functionalities can be incorporated into MOFs via organic linker functionalization,[44-47] entrapment of catalytically active species in pores/channels,[48-52] and more recently, transformation of metal-hydroxo/oxo nodes,[53-56] it is feasible to install multiple catalytic functionalities in MOFs via judicious combination of metal/metal-oxo nodes and functional organic ligand linkers followed by appropriate post-synthetic tranfromations.[57-63] The rigid, periodic, and porous structures of MOFs isolate disparate catalysts from each other, preventing their potential interference to afford truly orthogonal catalytic sites. However, due to the difficulty in characterizing MOFs after multistep functionalization, sequential engineering of multiple catalytic sites into MOFs has not been realized. Herein we report the first attempt at multi-step synthetic manipulations of an aluminum MOF to generate Lewis acid catalysts and Pd NPs for tandem catalytic hydrodeoxygenation of ethers, alcohols, and esters.

In this work, we targeted a mixed-ligand MOF (**1**) built from $(Al\text{-}OH)_n$ secondary building units (SBUs) and a mixture of 2,2'-bipyridine-5,5'-dicarboxylate(dcbpy) and 1,4-benzenediacrylate (pdac) ligands to install both Lewis acid and Pd NP active sites via multi-step synthetic manipulations (Scheme 1). The pdac ligands in **1** were selectively removed via post-synthetic ozonolysis to generate $Al_2(OH)(OH_2)$ sites. Subsequent triflation of $Al_2(OH)(OH_2)$ sites with trimethyl triflate (Me_3SiOTf) afforded strongly Lewis acidic sites for dehydroalkoxylation. Finally, coordination of $Pd(MeCN)_2Cl_2$ to dcbpy ligand followed by *in situ* reduction by hydrogen produced orthogonal Pd NP sites as the hydrogenation

catalyst. In-depth characterization of the MOFs after each post-synthetic manipulation supported selective and precise transformations to install orthogonal active sites in **1**-OTf-Pd^{NP}. The presence of both Lewis acid and Pd NP active sites in **1**-OTf-Pd^{NP} led to outstanding catalytic performance in apparent hydrogenolysis of etheric, alcoholic, and esteric C-O bonds to generate alkanes via a tandem dehydroalkoxylation-hydrogenation process under relatively mild conditions. The reactivity of C-O bonds followed the trend of tertiary carbon > secondary carbon > primary carbon. Control experiments confirmed the heterogeneous nature and recyclability of **1**-OTf-Pd^{NP} and its superior catalytic activity over the homogeneous counterparts.

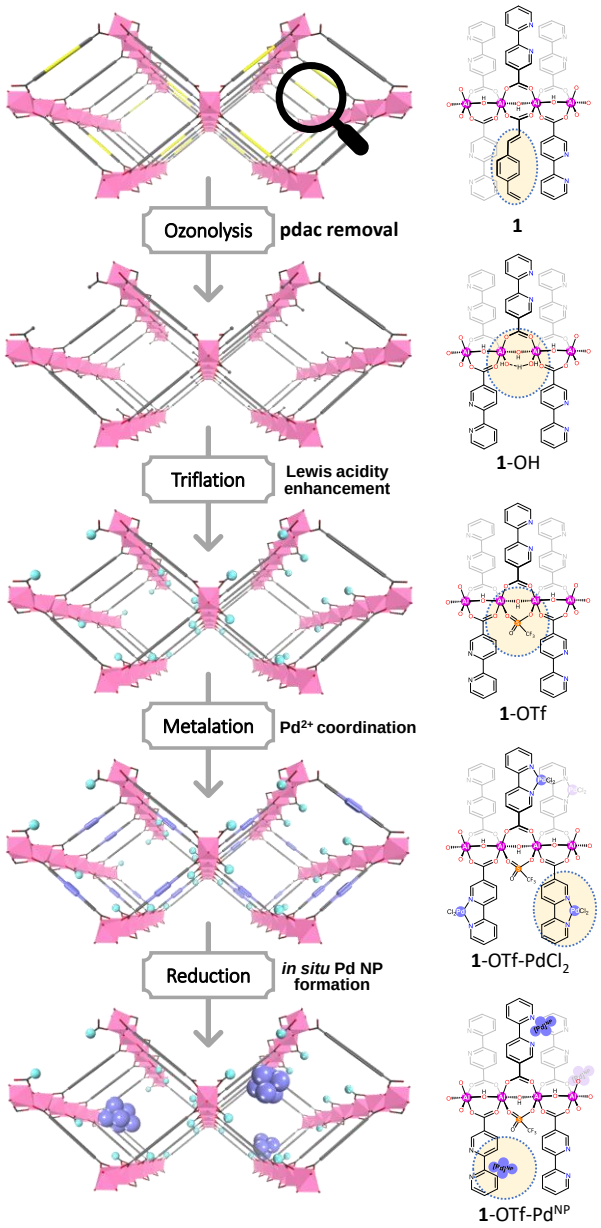

Scheme 1. Schematic showing sequential engineering of Lewis acid and Pd NP sites in **1**.

RESULTS AND DISCUSSION

Synthesis of Mixed-Ligand MOF 1 and Removal of pdac Ligands via Ozonolysis. The new MOF **1** with mixed dcbpy and pdac ligands based on DUT-5 structure was synthesized solvothermally by heating a mixture of $Al(NO_3)_3{\cdot}9H_2O$, dcbpy, pdac, and dimethylformamide (DMF) at 120 °C (Scheme S1, SI).[64-65] Powder X-ray diffraction (PXRD) studies revealed that **1** was isostructural to DUT-5 of the formula Al(OH)(bpdc) (bpdc = biphenyl-4,4'-dicarboxylate) and MOF-253 of the formula Al(OH)(dcbpy) (Figure 1c). The formula of **1** was determined as $Al(OH)(dcbpy)_{0.81}(pdac)_{0.19}$ based on ^{1}H NMR spectra of digested **1** (Figure S2, SI) and thermogravimetric analysis (TGA) of **1** (Figure S3, SI). Scanning electron microscopy (SEM) and transmission electron microscopy (TEM) imaging showed a plate-like morphology for **1** (Figure 1b, e), similar to that of DUT-5.[64] N_2 sorption measurements of **1** showed type I isotherms with a Brunauer-Emmett-Teller (BET) surface area of 1499 m^2/g, comparable to that of DUT-5 (1613 m^2/g, Figure 1d).

Post-synthetic transformations have recently been used to fine-tune micro- and meso-porosity of MOFs.[66-69] In particular, Maspoch and coworkers used ozonolysis to remove olefin-containing ligands from a mixed-ligand UiO-type MOF to afford both micro- and meso-porosity.[69] This ozonolysis process also removes some carboxylate ligands to generate $Al_2(OH)(OH_2)$ defect sites on the $(Al\text{-}OH)_n$ SBUs. We treated **1** with gaseous O_3 (0.42 mol/h @ 6 L/min O_2 flowing rate) to selectively remove the pdac ligands by cleaving the olefinic groups (Figure 1a, Scheme S2, SI). Further washing with DMF/HCl (1M) (10:1 v:v) removed the residual organic fragments trapped in the pores to afford **1**-OH with $Al_2(OH)(OH_2)$ defect sites as a white solid. ^{1}H NMR of digested **1**-OH revealed complete removal of pdac ligands during ozonolysis (Figure S5, SI). NMR and TGA analyses afforded a formula of $Al(OH)(dcbpy)_{0.81}(OH)_{0.38}(H_2O)_{0.38}$ for **1**-OH (Figure S6, SI). The crystallinity of **1** was maintained after ozonolysis as demonstrated by the similarity of PXRD patterns between **1** and **1**-OH (Figure 1c). TEM imaging showed that **1**-OH maintained the plate-like morphology of **1**, with evenly distributed spongy cleavages (Figure 1f). **1**-OH showed a BET surface area of 1190 m^2/g with the hysteresis characteristic of mesoporosity (Figure 1d). The removal of pdac ligands slightly reduced the BET surface area but increased pore sizes in the 13 - 32 Å range (Figure S7, SI). Ozonolysis of **1** thus generated mesopores which should facilitate substrate and product transport in catalytic reactions.

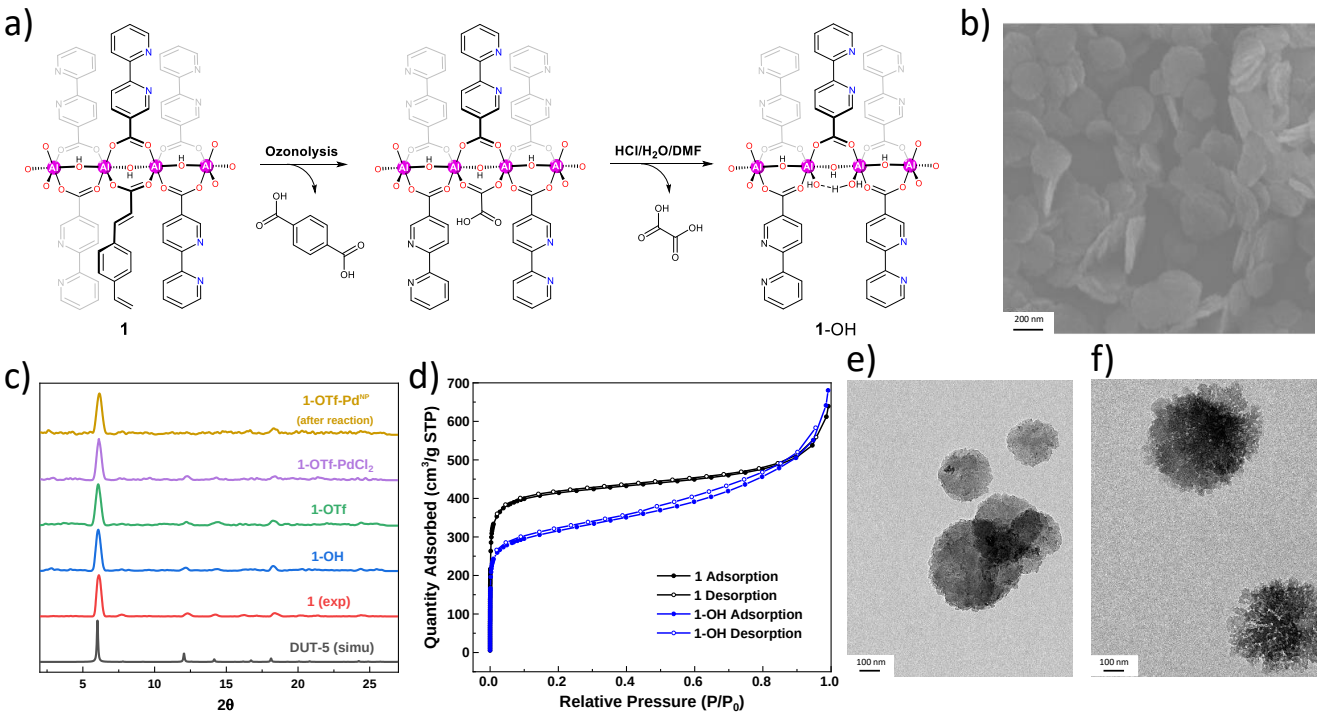

Figure 1. (a) Chemical equation showing ozonolysis of **1** followed by washing with DMF/HCl (1 M) to afford **1**-OH with $Al_2(OH)(OH_2)$ defect sites. (b) SEM image of as-synthesized **1**. (c) The similarity of PXRD patterns of **1** (red), **1**-OH (blue), **1**-OTf (green), **1**-OTf-$PdCl_2$ (purple), and **1**-OTf-Pd^{NP} (khaki) to the simulated pattern of DUT-5 (black) indicates the crystallinity of the MOF was maintained after multi-step post-synthetic manipulations. (d) N_2 sorption isotherms of **1** (black) and **1**-OH (blue). (e, f) TEM images of **1** (e) and **1**-OH (f).

Triflation of 1-OH and Lewis Acidity Determination for 1-OTf. Although MOF nodes have been widely used as Lewis acidic sites to catalyze organic transformations,[70-73] their Lewis acidity is significantly lower than the homogeneous benchmark $Sc(OTf)_3$. We recently developed a triflation strategy to significantly enhance Lewis acidity of MOF nodes.[74] **1**-OH was activated with Me_3SiOTf in benzene at room temperature for 12 h to afford **1**-OTf as a pale-yellow solid (Figure 2a). Me_3SiOTf quantitatively transformed $Al_2(OH)(OH_2)$ moieties to $Al_2(\mu_2\text{-OTf})$ sites due to the oxophilic nature of Me_3Si groups. ^{1}H NMR spectroscopy showed the generation of 1.93 equiv. of $(Me_3Si)_2O$ w.r.t. the $Al_2(OH)(OH_2)$ sites (Figure S8, SI), agreeing well with the expected value of 2 for the proposed activation process (Scheme S3, SI). Diffuse reflectance infrared Fourier transform spectroscopy (DRIFTS) supported the removal of $Al_2(OH)(OH_2)$ moieties. The increased absorption at 1231 – 1266 cm^{-1} in **1**-OTf corresponded to the $\nu(S{=}O^{OTf})$ band (Figure 2b, Figure S9a, SI). The sharp stretching band at 3708 cm^{-1} was observed for bridging μ_2-OH groups in both **1** and **1**-OH, [75] but this band shifted significantly to 3687 cm^{-1} for **1**-OTf (Figure 2b, Figure S9b, SI). Electron-withdrawing OTf groups weaken the O-H bonds of μ_2-OH groups in **1**-OTf, leading to a shift to lower energy. The broad peak centered at 3689 cm^{-1} in **1**-OH was attributed to hydrogen bonding interactions between neighboring Al-OH and Al-OH_2 moieties.[76]

We quantified Lewis acidity enhancement in **1**-OTf by electron paramagnetic resonance (EPR) spectroscopy of MOF-bound superoxide ($O_2^{\bullet-}$) and fluorescence spectroscopy of MOF-bound N-methylacridone (NMA).[74, 77] Superoxide radical ions ($O_2^{\bullet-}$) can be generated *in situ* by the 1e$^-$ reduction of O_2, which readily bind to Lewis acidic Al centers by displacing the weakly coordinating triflate groups to form EPR-active Al($O_2^{\bullet-}$) species (Figure S13b, SI). Coordination to Lewis acids significantly shifted the EPR signal of $O_2^{\bullet-}$, especially the g_{zz} tensor that is determined by energy splitting (ΔE) between the π_x^* and π_y^* orbitals.[78] **1**-OTf bound $O_2^{\bullet-}$ exhibited a g_{zz} of 2.032, which corresponds to a ΔE of 0.94 eV (Figure S13a, SI). In comparison, **1**-OH displayed a g_{zz} of 2.0352 with a corresponding ΔE of 0.85 eV. The 0.09 eV increase in ΔE makes **1**-OTf a much stronger Lewis acid and affords a more effective catalyst for C-O bond cleavage. Free NMA has an emission maximum (λ_{max}) at 433 nm when excited at 413 nm. Upon coordination to **1**-OTf, the Lewis acid adduct of NMA displayed a λ_{max} at 470 nm (Figure 2c, Figure S14, SI). The energy shift of NMA emission was previously established to be linearly related to the Lewis acidity of metal centers.[77, 79] Using the reported empirical equation, we calculated the ΔE value of **1**-OTf to be 0.93 eV, which is almost identical to the value measured by superoxide EPR spectroscopy. In comparison, **1**-OH only shifted the λ_{max} of NMA emission to 463 nm, with a calculated ΔE of 0.84 eV. Triflation of $Al_2(OH)(OH_2)$ moieties thus significantly enhanced Lewis acidity of **1**-OTf for catalytic applications.

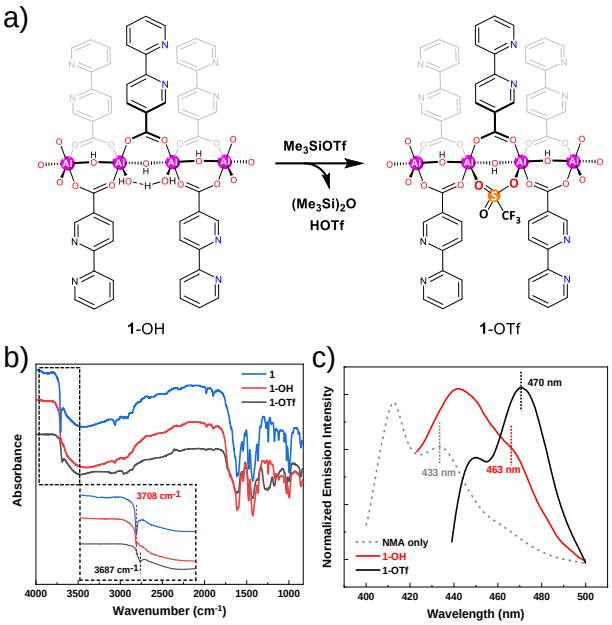

Figure 2. (a) Chemical equation showing triflation of **1**-OH to afford **1**-OTf. (b) DRIFT spectra of **1** (blue), **1**-OH (red), and **1**-OTf (black) show a significant shift of ν(μ_2-OH) from 3708 cm^{-1} (**1**, blue, and **1**-OH, red) to 3687 cm^{-1} (**1**-OTf, black). (c) Fluorescence spectra of **1**-OTf (black), **1**-OH (red), and free NMA (dashed).

Synthesis and Characterization of 1-OTf-PdCl$_2$ and 1-OTf-Pd^{NP}. **1**-OTf was further metalated with Pd(MeCN)$_2$Cl$_2$ in THF to afford the pre-catalyst **1**-OTf-PdCl$_2$ (Figure 3a, Scheme S4, SI). Inductively coupled plasma-mass spectrometry (ICP-MS) indicated an Al/Pd ratio of 2.10, corresponding to a formula of Al(OH)(dcbpy)$_{0.81}$(PdCl$_2$)$_{0.48}$(OTf)$_{0.38}$ for **1**-OTf-PdCl$_2$. This formula was supported by TGA analysis, which gave a residual weight of 27.8% (expected 28.6%) after ramping the temperature to 800 °C (Figure S11, SI). TEM imaging showed that **1**-OTf-PdCl$_2$ maintained the plate-like morphology of **1** (Figure S10, SI), whereas PXRD studies indicated that **1**-OTf-PdCl$_2$ maintained crystalline structure of **1** (Figure 1c). Pd coordination environment of **1**-OTf-PdCl$_2$ was studied by extended X-ray absorption fine structure (EXAFS) spectroscopy. The EXAFS data was collected at Pd K-edge and fitted with reported crystal structure of (bpy)PdCl$_2$ (Figure 3b).[80] The EXAFS feature of Pd centers in **1**-OTf-PdCl$_2$ was well fit with the structure to afford nearly identical coordination geometry and bond lengths (Figure 3d). Specifically, the Pd centers in **1**-OTf-PdCl$_2$ coordinate to two chlorides and one bpy ligand in a near square planar geometry with an average Pd-N bond length of 2.04 ± 0.01 Å and an average Pd-Cl bond length of 2.30 ± 0.02 Å (Table S1, SI). X-ray absorption near edge structure (XANES) spectroscopy showed that the Pd centers in **1**-OTf-PdCl$_2$ adopt +2 oxidation state (Figure S12).

Upon treatment with H$_2$ in the catalytic reaction, the Pd^{II} centers in **1**-OTf-PdCl$_2$ were readily reduced to form metallic Pd NPs in **1**-OTf-Pd^{NP}. To investigate the true catalytic active species during the reaction process, we characterized the MOF materials recovered from catalytic C-O cleavage reactions by PXRD, TEM, and XANES. PXRD studies showed that the MOF after catalysis remained crystalline (Figure 1c), whereas TEM imaging indicated the formation of Pd NPs which were dispersed evenly in the MOF matrix (Figure 3c). We further characterized the Pd^0 species in the recovered MOF by XANES. The recovered MOF showed XANES features corresponding to both Pd^0 and Pd^{II} species. We fitted the XANES spectra of **1**-OTf-Pd^{NP} with a linear combination of XANES spectra of PdCl$_2$ and Pd foil. The fitting gave ~48% Pd^0 species in the recovered MOF (Figure 3e); it is likely that surface Pd centers of **1**-OTf-Pd^{NP} were oxidized by air to afford Pd^{II} species when the samples were processed for XANES studies.

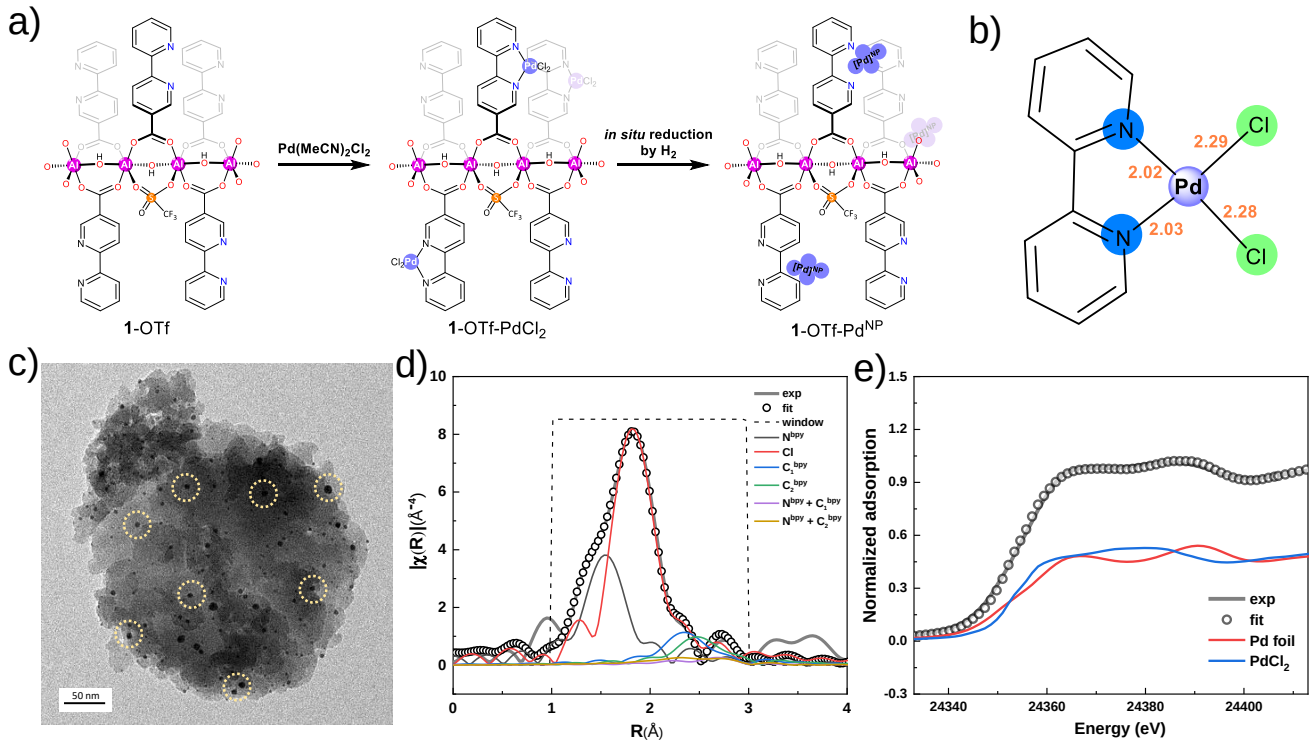

Figure 3. (a) Chemical equation showing metalation of **1**-OTf with Pd(MeCN)$_2$Cl$_2$ to afford **1**-OTf-PdCl$_2$ and *in situ* reduction of **1**-OTf-PdCl$_2$ to generate **1**-OTf-Pd^{NP}. (b) Fragment structure of (bpy)PdCl$_2$ for EXAFS fitting of the Pd coordination environment in **1**-OTf-PdCl$_2$. H atoms were omitted for clarity. (c) TEM image of **1**-OTf-Pd^{NP} shows evenly distributed Pd NPs in the MOF matrix after *in situ* reduction

in catalytic reactions. (d) EXAFS spectrum (gray solid line) and fit (black circles) in R-space at the Pd K-edge adsorption of **1**-OTf-$PdCl_2$. (e) Linear combination fitting of **1**-OTf-Pd^{NP} XANES feature using those of Pd foil and $PdCl_2$ as the basis functions.

1-OTf-$PdCl_2$ Catalyzed Tandem Ether/alcohol C-O Bond Cleavage. Etheric and alcoholic C-O linkages widely exist in biomass-based feedstocks. Their strong bonds present a major challenge for converting biomass into chemicals and hydrocarbon fuels with low oxygen contents.[12, 34, 81-85] Acids are shown to catalyze the C-O bond formation from hydroalkoxylation between alcohols and alkenes[74, 86-88] as well as its reversible process, dehydroalkoxylation to cleave an alkyl ether to form an olefin and an alcohol.[30-31, 35] As the dehydroalkoxylation process is endothermic with $\Delta H \approx$ 10~20 kcal/mol, its coupling with an exothermic alkene hydrogenation reaction makes the overall C-O bond cleavage reaction exothermic and produces a saturated alkane and an alcohol as the products.[30, 89] Multiple catalyst systems containing acid catalysts, such as homogeneous mineral acids and Lewis acids or heterogeneous acidic materials, and hydrogenation catalysts have been used to effect such a tandem process.[90-94] In particular, metal triflate salts and supported Pd catalysts effectively catalyzed ether and alcohol C-O bond hydrogenolysis to generate saturated hydrocarbons in a tandem manner.[30-31, 34] These catalyst systems tend to rapidly deactivate, require harsh conditions with elevated reaction temperatures and high H_2 pressures, and produce undesirable dimerized or aromatized byproducts. With isolated catalytic sites confined by the MOF framework, *in situ* generated **1**-OTf-Pd^{NP} catalyst is expected to significantly stabilize strongly Lewis acidic $Al_2(\mu_2\text{-OTf})$ sites and evenly distributed Pd NPs to realize highly effective tandem catalysis. At the same time, the pore restriction in the 1D channels of **1**-OTf-Pd^{NP} can prevent undesired dimerization and aromatization to improve product selectivity.

Table 1. Screening of reaction conditions for **1**-OTf-$PdCl_2$ Catalyzed Tandem Etheric/Alcohol C-O Bond Cleavage[a]

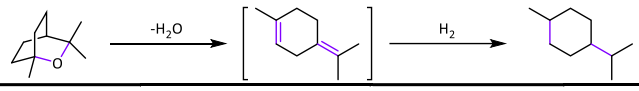

Entry	Catalyst (mol % Loading)	Solvent	Temp./ °C	Yield of menthane / %	TON
1	**1**-OTf-$PdCl_2$ (0.5%)	Octane	130	74	148
2	**1**-OTf-$PdCl_2$ (0.5%)	THF	130	31	62
3	**1**-OTf-$PdCl_2$ (0.1%)	neat	130	40	400
4	**1**-OTf-$PdCl_2$ (0.2%)	1,2-dichloroethane	100	>99	>500
5	**1**-OTf-$PdCl_2$ (0.1%)	1,2-dichloroethane	100	80	800
6	-	1,2-dichloroethane	100	N.D.	-
7[b]	**1**-OTf (0.2 %)	1,2-dichloroethane	100	<1	-
8[c]	**1**-OH-$PdCl_2$ (0.2 %)	1,2-dichloroethane	100	22	110
9[d]	$Al(OTf)_3$ + Pd (0.2 %)	1,2-dichloroethane	100	9	45
10[e]	HOTf + Pd (0.2 %)	1,2-dichloroethane	100	3	15

[a]Reaction conditions: **1**-OTf-$PdCl_2$ (loading w.r.t. $Al_2(\mu_2\text{-OTf})$, 0.6 mmol 1,8-cineole, 20 bar H_2, 1 mL solvent or neat condition, 24 h; Yield of menthane was determined by GC-MS analysis. [b]Catalysts: 0.2 mol% of **1**-OTf. [c]Catalysts: 0.2 mol% of **1**-OH-$PdCl_2$ (w.r.t. $Al_2(OH)(OH_2)$). [d]Catalysts: 0.2 mol% of $Al(OTf)_3$ + 0.25 mol% $Pd(MeCN)_2Cl_2$. [e]Catalysts: 0.2 mol% of HOTf + 0.25 mol% $Pd(MeCN)_2Cl_2$.

1,8-cinole was used as a model compound to optimize the reaction conditions for tandem C-O bond cleavage (Table 1). Initial screening of solvents revealed that 1,8-cinole could be quantitatively converted to menthane in 1,2-dichloroethane at 0.2 mol% loading of **1**-OTf-$PdCl_2$ [w.r.t. Lewis acidic $Al_2(\mu_2\text{-OTf})$ sites] and 100 °C under 20 bar of H_2 for 24 h. Nonpolar solvents such as octane and coordinating solvents such as THF gave lower catalytic performance, likely due to poor substrate solubility and poisoning of Lewis acidic metal sites, respectively. The highest TON of 800 was obtained when the catalyst loading was lowered to 0.1 mol%; this level of catalytic activity significantly outperformed previously reported catalytic systems. **1**-OTf-$PdCl_2$ is also advantageous to the well-studied homogeneous metal triflate plus supported Pd NP system by avoiding the use of substoichiometric amounts of expensive metal triflates such as $Hf(OTf)_4$, $Sc(OTf)_3$, and $Yb(OTf)_3$.

Several control experiments were conducted to gain insights into the tandem catalytic pathway of **1**-OTf-$PdCl_2$ mediated C-O bond cleavage. In the absence of the MOF catalyst, 1,8-cinole was totally unreactive under the reaction condition (Table 1, entry 6). At a loading of 0.2 mol% **1**-OTf, a negligible amount of menthane was detected (Table 1, entry 7). The lack of activity of **1**-OTf is likely due to the unfavorable thermodynamics of the dehydroalkoxylation reaction. 0.2 mol% loading of **1**-OH-$PdCl_2$ gave a much lower menthane yield of 22% (Table 1, entry 8), consistent with much lower Lewis acidity of $Al_2(OH)(OH_2)$ sites than $Al_2(\mu_2\text{-OTf})$ sites. Under identical conditions, homogenous controls with $Al(OTf)_3$ plus $Pd(MeCN)_2Cl_2$ and HOTf plus $Pd(MeCN)_2Cl_2$ gave very low menthane yields of 9% and 3%, respectvely (Table 1, entries 9 and 10). These results suggest that C-O bond cleavage by **1**-OTf-$PdCl_2$ occurs in a tandem manner, where strong Lewis acidic $Al_2(\mu_2\text{-OTf})$ sites on the SBUs catalyze the dehydroalkoxylation of etheric/alcoholic C-O bonds to afford C=C bonds which are hydrogenated by nearby Pd NPs confined in the MOF channels. The hydrogenation reaction pushes the equilibrium to the right to form saturated hydrocarbons (Figure 4a).

We next examined the substrate scope of **1**-OTf-$PdCl_2$ catalyzed tandem etheric/alcoholic C-O bond cleavage. A broad scope of substrates including tertiary (3°), secondary (2°), and primary (1°) alcohols/ethers were readily converted to alkanes by **1**-OTf-$PdCl_2$ under similar conditions (Table 2). Quantitative conversion of 3° alcohol (1-methylcyclohexanol) and 3° ether (1,8-cineole) to saturated alkanes was achieved at 0.1-0.2 mol% loading of **1**-OTf-$PdCl_2$ and at 100 °C (Table 2, entries 1 and 2). Reaction temperatures as high as 150 °C were needed to quantitatively convert 2° alcohols and ethers (cyclohexanol, 2-octanol, dicyclohexyl ether, and cyclohexyl phenyl ether) to corresponding saturated alkanes (Table 2, entries 4-7). 1° alcohol (1-heptanol) required even higher reaction temperatures of up to 200 °C and 0.5 mol% loading of **1**-OTf-$PdCl_2$ to afford heptane in 92% yield (Table 2, entry 8). High product selectivity was observed for different kinds of substrates with **1**-OTf-$PdCl_2$ as the catalyst without detection of any undesired dimerization or aromatization product. The outstanding product selectivity of **1**-OTf-$PdCl_2$ is attributed to the pore size exclusion by the uniform MOF channels and well-defined, site-isolated Lewis acids and Pd NPs in the MOF. Notably, 1° ethers with active

β-hydrogen atoms, i.e., phenethoxybenzene and (2-methoxyethyl)benzene, underwent C-O bond cleavage at 150 °C and 130 °C, respectively, to produce ethylbenzene as the main product with a high selectivity over the over-hydrogenated product methylcyclohexane.

Table 2. Substrate Scope for **1**-OTf-$PdCl_2$ Catalyzed Tandem Etheric/Alcoholic C-O Bond Cleavage[a]

Entry	Substrate	Catalyst Loading	Reaction Temperature	Product	Conversion (Yield)
1		0.1 mol%	100 °C		100% (>99%)
2		0.2 mol%	100 °C		100% (>99%)
3		0.1 mol%	100 °C		80% (80%)
4		0.1 mol%	150 °C		100% (>99%)
5	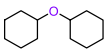	0.1 mol%	150 °C		100% (97%)
6	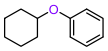	0.1 mol%	150 °C		94% (89%)[b]
7	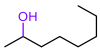	0.2 mol%	150 °C	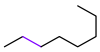	100% (>99%)
8	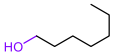	0.5 mol%	200 °C		100% (92%)
9	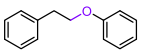	0.2 mol%	150 °C		100% (89%)[b]
10	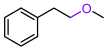	0.2 mol%	130 °C		70% (61%)[b]

[a]Unless noted, all reactions performed with indicated amount of **1**-OTf-$PdCl_2$, 0.6 mmol of substrate, and 20 bar H_2 in 1.0 mL of 1,2-dichloroethane for 24 h. Conversions and yields determined by GC-MS integrals with mesitylene as the internal standard. See Table S4, SI for details and isolated yields for select products. [b]Reaction performed in 1 bar H_2.

Several lines of evidence support the heterogeneity of **1**-OTf-$PdCl_2$ in tandem C-O bond cleavage reactions. The catalysts recovered from C-O bond cleavage reactions exhibited identical PXRD patterns to pristine **1**, indicating structural stability of **1**-OTf-$PdCl_2$ in catalytic reactions (Figure 1c). Lewis acidity quantification on the MOF recovered from the catalytic reaction confirmed the maintenance of Lewis acidity in the catalytic process (Figure S15, SI). ICP-MS analysis showed minimal leaching of Al (0.6%) and Pd (0.02%) into the supernatant after the first reaction run whereas ^{19}F NMR analysis indicated negligible leaching of OTf into the supernatant after catalysis (Figure S19, SI). "Hot filtration" test was also carried out to further exclude the possibility of soluble metal or acid species contributing to the catalytic performance (Figure S18, SI). After the reaction was interrupted, the solution phase and the solid phase were separated and used, respectively, for another reaction run. The recovered solid retained the catalytic activity but the solution was totally inactive, proving the heterogeneity of **1**-OTf-$PdCl_2$. Impressively, **1**-OTf-$PdCl_2$ was readily recovered by simple centrifugation and reused for at least 5 times without significant drop in catalytic activity (Figure 4b). Moreover, **1**-OTf-$PdCl_2$ catalyzed tandem C-O cleavage of 1,8-cinole at ~2 g scale (20 times larger scale) afforded menthane in 75% yield in 24 h under standard reaction conditions. The excellent thermal stability and recyclability make **1**-OTf-$PdCl_2$ a potential candidate catalyst for practical tandem etheric/alcoholic C-O bond cleavage.

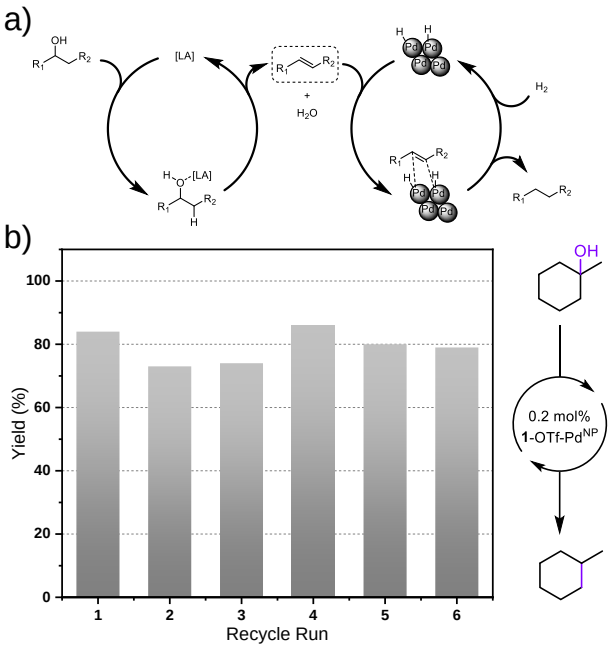

Figure 4. (a) Proposed tandem pathway for **1**-OTf-$PdCl_2$-mediated C-O bond cleavage. (b) Recycle experiments for **1**-OTf-$PdCl_2$ catalyzed C-O bond cleavage of 1-methylcyclohexanol. Plots of methylcyclohexane yields (%) in six consecutive runs with 3 h of reaction time.

1-OTf-$PdCl_2$ Catalyzed Tandem Ester C-O Bond Cleavage. Ester groups also widely exist in bio-derived molecules such as triglycerides, fats, and oils, which provide a source of renewable diesel after their decarboxylation.[95-97] Traditional decarboxylation methods require high temperatures of up to 500 °C to thermally crack the C-O bond followed by CO_2 release.[98-101] Metal triflates plus Pd/C have recently been used to catalyze tandem ester C-O bond cleavage with moderate to good selectivity and yields.[32-33, 102]

1-OTf-$PdCl_2$ was also proved highly active for tandem ester C-O bond cleavage with a reactivity trend of 3° carbon > 2° carbon > 1° carbon (Table 3). The 3° ester terpinyl acetate was effectively cleaved to produce menthane at 0.2 mol% loading of **1**-OTf-$PdCl_2$ at 100 °C, affording a TON of 440 (Table 3, entry 1). The 2° ester L-menthyl acetate was decarboxylated in the presence of 0.5 mol% **1**-OTf-$PdCl_2$ at 150 °C to afford menthane in quantitative yield (Table 3, entry 2). Other 2° acetate or propionate esters, i.e., cyclohexyl acetate, and cyclohexyl propionate, readily underwent C-O cleavage at 0.5 mol% **1**-OTf-$PdCl_2$ at 150 °C to afford decarboxylated products in 62 to 84% yields (Table 3, entries 4-5). For the 1° ester octyl acetate, a higher temperate of 200 °C was needed to afford octane in 79% yield (Table 3, entry 6). Interestingly, 1° ester with active β-hydrogen atoms, i.e., phenethyl acetate, readily underwent C-O cleavage at 0.2 mol% loading of **1**-OTf-$PdCl_2$ and 130 °C to afford ethylbenzene in 94% yield (Table 3, entry 7). Moreover, the lactone·5-hexanolide also underwent tandem C-O cleavage to generate the saturated carboxylic acid (hexanoic acid) in 61% yield (Table 3, entry 8). Such a MOF-based tandem catalyst system thus provided a potent solution for cleavage of esteric C-O bonds.

Table 3. Substrate Scope for **1**-OTf-$PdCl_2$ Catalyzed Ester C-O Bond Cleavage[a]

Entry	Substrate	Catalyst Loading	Reaction Temperature	Product	Conversion (Yield)
1	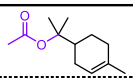	0.2 mol%	100 °C		100% (88%)[b]
2	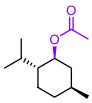	0.5 mol%	150 °C		100% (>99%)
3		0.1 mol%	150 °C		45% (45%)
4		0.5 mol%	150 °C		91% (84%)[b]
5	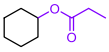	0.5 mol%	150 °C		87% (62%)[b]
6		0.5 mol%	200 °C		100% (79%)
7	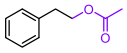	0.2 mol%	130 °C		100% (94%)[c]
8		0.2 mol%	130 °C		100% (61%)

[a]Unless noted, all reactions performed with indicated amount of **1**-OTf-$PdCl_2$, 0.6 mmol of substrate, and 20 bar H_2 in 1.0 mL of 1,2-dichloroethane for 24 h. Conversions and yields determined by GC-MS integrals with mesitylene as the internal standard. See Table S5, SI for details and isolated yields for select products. [b]Reaction performed for 36 h. [c]Reaction performed in 1 bar H_2 for 6 h.

CONCLUSION

In this work, we demonstrated hierarchical installation of orthogonal Lewis acid and Pd NP catalysts on a mixed-ligand MOF via multi-step sequential transformations. The pdac ligands in **1** were first removed via ozonolysis to generate $Al_2(OH)(OH_2)$ defect sites in the infinite chain-like $[Al(\mu_2\text{-}OH)]_n$ SBUs of **1**, which were subsequently triflated to afford strongly Lewis acidic **1**-OTf. Coordination of dcbpy ligands in **1**-OTf with $Pd(MeCN)_2Cl_2$ followed *in situ* H_2 reduction afforded multi-catalytic MOF **1**-OTf-Pd^{NP} for tandem dehydroalkoxylation-hydrogenation of etheric, alcoholic, and esteric C-O bonds to generate saturated alkanes under relatively mild conditions. **1**-OTf-Pd^{NP} exhibit C-O bond cleavage activity trend of tertiary carbon > secondary carbon > primary carbon and could be readily reused via simple solid/liquid separation. **1**-OTf-Pd^{NP} showed superior catalytic activity over the homogeneous counterparts owing to hierarchical incorporation of orthogonal Lewis acid and Pd NP active sites. Our work shows the potential of sequential engineering of multiple catalytic sites in MOFs in addressing outstanding challenges in sustainable catalysis.

ASSOCIATED CONTENT

Supporting Information

This material is available free of charge via the Internet at http://pubs.acs.org.; Synthesis and characterization of **1**, **1**-OH, **1**-OTf, **1**-OTf-$PdCl_2$, and **1**-OTf-Pd^{NP}; reaction procedures and evaluation of catalytic performance.

AUTHOR INFORMATION

† Y. Song and X. Feng contributed equally to this work.

Corresponding Author Email: wenbinlin@uchicago.edu

ORCID

ACKNOWLEDGMENT

This work was supported by NSF (CHE-1464941) and the University of Chicago. We thank Mr. Xiaomin Jiang and Mr. Taokun Luo for experimental help. We thank Mr. Lingbowei Hu and Dr. Viresh Rawal for the help with ozonolysis. XAS analysis was performed at Beamline 10-BM, supported by the Materials Research Collaborative Access Team (MRCAT). Use of the Advanced Photon Source, an Office of Science User Facility operated for the U.S. DOE Office of Science by ANL, was supported by the U.S. DOE under Contract No. DE-AC02-06CH11357.

References

1. Zakzeski, J.; Bruijnincx, P. C. A.; Jongerius, A. L.; Weckhuysen, B. M., The Catalytic Valorization of Lignin for the Production of Renewable Chemicals. *Chem. Rev.* **2010,** *110* (6), 3552-3599.
2. Azadi, P.; Inderwildi, O. R.; Farnood, R.; King, D. A., Liquid fuels, hydrogen and chemicals from lignin: A critical review. *Renew. Sustain. Energy Rev.* **2013,** *21*, 506-523.
3. Ragauskas, A. J.; Beckham, G. T.; Biddy, M. J.; Chandra, R.; Chen, F.; Davis, M. F.; Davison, B. H.; Dixon, R. A.; Gilna, P.; Keller, M.; Langan, P.; Naskar, A. K.; Saddler, J. N.; Tschaplinski, T. J.; Tuskan, G. A.; Wyman, C. E., Lignin Valorization: Improving Lignin Processing in the Biorefinery. *Science* **2014,** *344* (6185), 1246843.
4. Corma, A.; Iborra, S.; Velty, A., Chemical Routes for the Transformation of Biomass into Chemicals. *Chem. Rev.* **2007,** *107* (6), 2411-2502.
5. Sheldon, R. A., Utilisation of biomass for sustainable fuels and chemicals: Molecules, methods and metrics. *Catal. Today* **2011,** *167* (1), 3-13.
6. Tuck, C. O.; Pérez, E.; Horváth, I. T.; Sheldon, R. A.; Poliakoff, M., Valorization of Biomass: Deriving More Value from Waste. *Science* **2012,** *337* (6095), 695.
7. Deuss, P. J.; Barta, K.; de Vries, J. G., Homogeneous catalysis for the conversion of biomass and biomass-derived platform chemicals. *Catal. Sci. Technol.* **2014,** *4* (5), 1174-1196.
8. Asomaning, J.; Haupt, S.; Chae, M.; Bressler, D. C., Recent developments in microwave-assisted thermal conversion of biomass for fuels and chemicals. *Renew. Sustain. Energy Rev.* **2018,** *92*, 642-657.
9. Ragauskas, A. J.; Williams, C. K.; Davison, B. H.; Britovsek, G.; Cairney, J.; Eckert, C. A.; Frederick, W. J.; Hallett, J. P.; Leak, D. J.; Liotta, C. L.; Mielenz, J. R.; Murphy, R.; Templer, R.; Tschaplinski, T., The Path Forward for Biofuels and Biomaterials. *Science* **2006,** *311* (5760), 484.
10. Matson, T. D.; Barta, K.; Iretskii, A. V.; Ford, P. C., One-Pot Catalytic Conversion of Cellulose and of Woody Biomass Solids to Liquid Fuels. *J. Am. Chem. Soc.* **2011,** *133* (35), 14090-14097.
11. Sanderson, K., Lignocellulose: A chewy problem. *Nature* **2011,** *474* (7352), S12-S14.
12. Swain, P. K.; Das, L. M.; Naik, S. N., Biomass to liquid: A prospective challenge to research and development in 21st century. *Renew. Sustain. Energy Rev.* **2011,** *15* (9), 4917-4933.
13. Bruijnincx, P. C. A.; Weckhuysen, B. M., Lignin up for break-down. *Nat. Chem.* **2014,** *6* (12), 1035-1036.
14. Xie, H.; Gathergood, N., *The role of green chemistry in biomass processing and conversion*. Wiley Online Library: 2013.
15. Yan, N.; Zhao, C.; Dyson, P. J.; Wang, C.; Liu, L.-t.; Kou, Y., Selective Degradation of Wood Lignin over Noble-Metal Catalysts in a Two-Step Process. *ChemSusChem* **2008,** *1* (7), 626-629.
16. Sergeev, A. G.; Hartwig, J. F., Selective, Nickel-Catalyzed Hydrogenolysis of Aryl Ethers. *Science* **2011,** *332*

(6028), 439.
17. Zhao, C.; Lercher, J. A., Selective Hydrodeoxygenation of Lignin-Derived Phenolic Monomers and Dimers to Cycloalkanes on Pd/C and HZSM-5 Catalysts. *ChemCatChem* **2012,** *4* (1), 64-68.
18. Sergeev, A. G.; Webb, J. D.; Hartwig, J. F., A Heterogeneous Nickel Catalyst for the Hydrogenolysis of Aryl Ethers without Arene Hydrogenation. *J. Am. Chem. Soc.* **2012,** *134* (50), 20226-20229.
19. Song, Q.; Wang, F.; Xu, J., Hydrogenolysis of lignosulfonate into phenols over heterogeneous nickel catalysts. *Chem. Commun.* **2012,** *48* (56), 7019-7021.
20. He, J.; Zhao, C.; Lercher, J. A., Ni-Catalyzed Cleavage of Aryl Ethers in the Aqueous Phase. *J. Am. Chem. Soc.* **2012,** *134* (51), 20768-20775.
21. Zhang, J.; Teo, J.; Chen, X.; Asakura, H.; Tanaka, T.; Teramura, K.; Yan, N., A Series of NiM (M = Ru, Rh, and Pd) Bimetallic Catalysts for Effective Lignin Hydrogenolysis in Water. *ACS Catal.* **2014,** *4* (5), 1574-1583.
22. Molinari, V.; Giordano, C.; Antonietti, M.; Esposito, D., Titanium Nitride-Nickel Nanocomposite as Heterogeneous Catalyst for the Hydrogenolysis of Aryl Ethers. *J. Am. Chem. Soc.* **2014,** *136* (5), 1758-1761.
23. Zaheer, M.; Hermannsdörfer, J.; Kretschmer, W. P.; Motz, G.; Kempe, R., Robust Heterogeneous Nickel Catalysts with Tailored Porosity for the Selective Hydrogenolysis of Aryl Ethers. *ChemCatChem* **2014,** *6* (1), 91-95.
24. Luo, H.; Klein, I. M.; Jiang, Y.; Zhu, H.; Liu, B.; Kenttämaa, H. I.; Abu-Omar, M. M., Total Utilization of Miscanthus Biomass, Lignin and Carbohydrates, Using Earth Abundant Nickel Catalyst. *ACS Sustainable Chemistry & Engineering* **2016,** *4* (4), 2316-2322.
25. Song, Y.; Li, Z.; Ji, P.; Kaufmann, M.; Feng, X.; Chen, J. S.; Wang, C.; Lin, W., Metal–Organic Framework Nodes Support Single-Site Nickel(II) Hydride Catalysts for the Hydrogenolysis of Aryl Ethers. *ACS Catal.* **2019,** *9* (2), 1578-1583.
26. Huang, H.; Denard, C. A.; Alamillo, R.; Crisci, A. J.; Miao, Y.; Dumesic, J. A.; Scott, S. L.; Zhao, H., Tandem Catalytic Conversion of Glucose to 5-Hydroxymethylfurfural with an Immobilized Enzyme and a Solid Acid. *ACS Catal.* **2014,** *4* (7), 2165-2168.
27. Orazov, M.; Davis, M. E., Tandem catalysis for the production of alkyl lactates from ketohexoses at moderate temperatures. *Proc. Natl. Acad. Sci. U.S.A* **2015,** *112* (38), 11777.
28. Yang, X.; Li, T.; Tang, K.; Zhou, X.; Lu, M.; Ounkham, W. L.; Spain, S. M.; Frost, B. J.; Lin, H., Highly efficient conversion of terpenoid biomass to jet-fuel range cycloalkanes in a biphasic tandem catalytic process. *Green Chem.* **2017,** *19* (15), 3566-3573.
29. Yang, M.; Qi, H.; Liu, F.; Ren, Y.; Pan, X.; Zhang, L.; Liu, X.; Wang, H.; Pang, J.; Zheng, M.; Wang, A.; Zhang, T., One-Pot Production of Cellulosic Ethanol via Tandem Catalysis over a Multifunctional Mo/Pt/WOx Catalyst. *Joule* **2019,** *3* (8), 1937-1948.
30. Atesin, A. C.; Ray, N. A.; Stair, P. C.; Marks, T. J., Etheric C–O Bond Hydrogenolysis Using a Tandem Lanthanide Triflate/Supported Palladium Nanoparticle Catalyst System. *J. Am. Chem. Soc.* **2012,** *134* (36), 14682-14685.
31. Li, Z.; Assary, R. S.; Atesin, A. C.; Curtiss, L. A.; Marks, T. J., Rapid Ether and Alcohol C–O Bond Hydrogenolysis Catalyzed by Tandem High-Valent Metal Triflate + Supported Pd Catalysts. *J. Am. Chem. Soc.* **2014,** *136* (1), 104-107.
32. Lohr, T. L.; Li, Z.; Marks, T. J., Selective Ether/Ester C–O Cleavage of an Acetylated Lignin Model via Tandem Catalysis. *ACS Catal.* **2015,** *5* (11), 7004-7007.
33. Lohr, T. L.; Li, Z.; Assary, R. S.; Curtiss, L. A.; Marks, T. J., Thermodynamically Leveraged Tandem Catalysis for Ester RC(O)O − R′ Bond Hydrogenolysis. Scope and Mechanism. *ACS Catal.* **2015,** *5* (6), 3675-3679.
34. Lohr, T. L.; Li, Z.; Marks, T. J., Thermodynamic Strategies for C–O Bond Formation and Cleavage via Tandem Catalysis. *Acc. Chem. Res.* **2016,** *49* (5), 824-834.
35. Assary, R. S.; Atesin, A. C.; Li, Z.; Curtiss, L. A.; Marks, T. J., Reaction Pathways and Energetics of Etheric C–O Bond Cleavage Catalyzed by Lanthanide Triflates. *ACS Catal.* **2013,** *3* (9), 1908-1914.
36. Yoshikai, N.; Matsuda, H.; Nakamura, E., Hydroxyphosphine Ligand for Nickel-Catalyzed Cross-Coupling through Nickel/Magnesium Bimetallic Cooperation. *J. Am. Chem. Soc.* **2009,** *131* (27), 9590-9599.
37. Cui, M.; Qian, Q.; He, Z.; Zhang, Z.; Ma, J.; Wu, T.; Yang, G.; Han, B., Bromide promoted hydrogenation of CO2 to higher alcohols using Ru–Co homogeneous catalyst. *Chem. Sci.* **2016,** *7* (8), 5200-5205.
38. Li, R.; Zhou, Y.; Xu, X.; Dong, G., Direct Vicinal Difunctionalization of Thiophenes Enabled by the Palladium/Norbornene Cooperative Catalysis. *J. Am. Chem. Soc.* **2019,** *141* (48), 18958-18963.
39. Ma, L.; Abney, C.; Lin, W., Enantioselective catalysis with homochiral metal–organic frameworks. *Chem. Soc. Rev.* **2009,** *38* (5), 1248-1256.
40. Lee, J.; Farha, O. K.; Roberts, J.; Scheidt, K. A.; Nguyen, S. T.; Hupp, J. T., Metal–organic framework materials as catalysts. *Chem. Soc. Rev.* **2009,** *38* (5), 1450-1459.
41. Yoon, M.; Srirambalaji, R.; Kim, K., Homochiral Metal–Organic Frameworks for Asymmetric Heterogeneous Catalysis. *Chem. Rev.* **2012,** *112* (2), 1196-1231.
42. Liu, J.; Chen, L.; Cui, H.; Zhang, J.; Zhang, L.; Su, C.-Y., Applications of metal–organic frameworks in heterogeneous supramolecular catalysis. *Chem. Soc. Rev.* **2014,** *43* (16), 6011-6061.
43. Jiao, L.; Wang, Y.; Jiang, H.-L.; Xu, Q., Metal–Organic Frameworks as Platforms for Catalytic Applications. *Adv. Mater.* **2018,** *30* (37), 1703663.
44. Ma, L.; Falkowski, J. M.; Abney, C.; Lin, W., A series of isoreticular chiral metal–organic frameworks as a tunable platform for asymmetric catalysis. *Nat. Chem.* **2010,** *2* (10), 838-846.
45. Cohen, S. M., Postsynthetic Methods for the Functionalization of Metal–Organic Frameworks. *Chem. Rev.* **2012,** *112* (2), 970-1000.
46. Zhao, M.; Ou, S.; Wu, C.-D., Porous Metal–Organic Frameworks for Heterogeneous Biomimetic Catalysis. *Acc. Chem. Res.* **2014,** *47* (4), 1199-1207.
47. Feng, L.; Wang, Y.; Yuan, S.; Wang, K.-Y.; Li, J.-L.; Day, G. S.; Qiu, D.; Cheng, L.; Chen, W.-M.; Madrahimov, S. T.; Zhou, H.-C., Porphyrinic Metal–Organic Frameworks Installed with Brønsted Acid Sites for Efficient Tandem Semisynthesis of Artemisinin. *ACS Catal.* **2019,** *9* (6), 5111-5118.
48. Huang, Y.; Zhang, Y.; Chen, X.; Wu, D.; Yi, Z.; Cao, R., Bimetallic alloy nanocrystals encapsulated in ZIF-8 for synergistic catalysis of ethylene oxidative degradation. *Chem. Commun.* **2014,** *50* (70), 10115-10117.
49. Na, K.; Choi, K. M.; Yaghi, O. M.; Somorjai, G. A., Metal Nanocrystals Embedded in Single Nanocrystals of MOFs Give Unusual Selectivity as Heterogeneous Catalysts. *Nano Lett.* **2014,** *14* (10), 5979-5983.
50. Shen, L.; Luo, M.; Huang, L.; Feng, P.; Wu, L., A Clean and General Strategy To Decorate a Titanium Metal–Organic Framework with Noble-Metal Nanoparticles for Versatile Photocatalytic Applications. *Inorg. Chem.* **2015,** *54* (4), 1191-1193.
51. Li, X.; Goh, T. W.; Li, L.; Xiao, C.; Guo, Z.; Zeng, X. C.; Huang, W., Controlling Catalytic Properties of Pd Nanoclusters through Their Chemical Environment at the Atomic Level Using Isoreticular Metal–Organic Frameworks. *ACS Catal.* **2016,** *6* (6), 3461-3468.
52. Zhao, M.; Yuan, K.; Wang, Y.; Li, G.; Guo, J.; Gu, L.;

Hu, W.; Zhao, H.; Tang, Z., Metal–organic frameworks as selectivity regulators for hydrogenation reactions. *Nature* **2016,** *539* (7627), 76-80.
53. Xiao, D. J.; Bloch, E. D.; Mason, J. A.; Queen, W. L.; Hudson, M. R.; Planas, N.; Borycz, J.; Dzubak, A. L.; Verma, P.; Lee, K.; Bonino, F.; Crocellà, V.; Yano, J.; Bordiga, S.; Truhlar, D. G.; Gagliardi, L.; Brown, C. M.; Long, J. R., Oxidation of ethane to ethanol by N2O in a metal–organic framework with coordinatively unsaturated iron(II) sites. *Nat. Chem.* **2014,** *6* (7), 590-595.
54. Nguyen, H. G. T.; Schweitzer, N. M.; Chang, C.-Y.; Drake, T. L.; So, M. C.; Stair, P. C.; Farha, O. K.; Hupp, J. T.; Nguyen, S. T., Vanadium-Node-Functionalized UiO-66: A Thermally Stable MOF-Supported Catalyst for the Gas-Phase Oxidative Dehydrogenation of Cyclohexene. *ACS Catal.* **2014,** *4* (8), 2496-2500.
55. Comito, R. J.; Fritzsching, K. J.; Sundell, B. J.; Schmidt-Rohr, K.; Dincă, M., Single-Site Heterogeneous Catalysts for Olefin Polymerization Enabled by Cation Exchange in a Metal-Organic Framework. *J. Am. Chem. Soc.* **2016,** *138* (32), 10232-10237.
56. Manna, K.; Ji, P.; Lin, Z.; Greene, F. X.; Urban, A.; Thacker, N. C.; Lin, W., Chemoselective single-site Earth-abundant metal catalysts at metal–organic framework nodes. *Nat. Commun.* **2016,** *7* (1), 12610.
57. Pan, Y.; Yuan, B.; Li, Y.; He, D., Multifunctional catalysis by Pd@MIL-101: one-step synthesis of methyl isobutyl ketone over palladium nanoparticles deposited on a metal–organic framework. *Chem. Commun.* **2010,** *46* (13), 2280-2282.
58. Song, F.; Wang, C.; Lin, W., A chiral metal–organic framework for sequential asymmetric catalysis. *Chem. Commun.* **2011,** *47* (29), 8256-8258.
59. Vermoortele, F.; Ameloot, R.; Vimont, A.; Serre, C.; De Vos, D., An amino-modified Zr-terephthalate metal–organic framework as an acid–base catalyst for cross-aldol condensation. *Chem. Commun.* **2011,** *47* (5), 1521-1523.
60. Park, J.; Li, J.-R.; Chen, Y.-P.; Yu, J.; Yakovenko, A. A.; Wang, Z. U.; Sun, L.-B.; Balbuena, P. B.; Zhou, H.-C., A versatile metal–organic framework for carbon dioxide capture and cooperative catalysis. *Chem. Commun.* **2012,** *48* (80), 9995-9997.
61. Pintado-Sierra, M.; Rasero-Almansa, A. M.; Corma, A.; Iglesias, M.; Sánchez, F., Bifunctional iridium-(2-aminoterephthalate)–Zr-MOF chemoselective catalyst for the synthesis of secondary amines by one-pot three-step cascade reaction. *J. Catal.* **2013,** *299*, 137-145.
62. Jiang, Z.-R.; Wang, H.; Hu, Y.; Lu, J.; Jiang, H.-L., Polar Group and Defect Engineering in a Metal–Organic Framework: Synergistic Promotion of Carbon Dioxide Sorption and Conversion. *ChemSusChem* **2015,** *8* (5), 878-885.
63. Huang, Y.-B.; Liang, J.; Wang, X.-S.; Cao, R., Multifunctional metal–organic framework catalysts: synergistic catalysis and tandem reactions. *Chem. Soc. Rev.* **2017,** *46* (1), 126-157.
64. Senkovska, I.; Hoffmann, F.; Fröba, M.; Getzschmann, J.; Böhlmann, W.; Kaskel, S., New highly porous aluminium based metal-organic frameworks: Al(OH)(ndc) (ndc=2,6-naphthalene dicarboxylate) and Al(OH)(bpdc) (bpdc=4,4′-biphenyl dicarboxylate). *Microporous Mesoporous Mater.* **2009,** *122* (1), 93-98.
65. Bloch, E. D.; Britt, D.; Lee, C.; Doonan, C. J.; Uribe-Romo, F. J.; Furukawa, H.; Long, J. R.; Yaghi, O. M., Metal Insertion in a Microporous Metal−Organic Framework Lined with 2,2′-Bipyridine. *J. Am. Chem. Soc.* **2010,** *132* (41), 14382-14384.
66. Tu, B.; Pang, Q.; Wu, D.; Song, Y.; Weng, L.; Li, Q., Ordered Vacancies and Their Chemistry in Metal–Organic Frameworks. *J. Am. Chem. Soc.* **2014,** *136* (41), 14465-14471.
67. Kim, Y.; Yang, T.; Yun, G.; Ghasemian, M. B.; Koo, J.; Lee, E.; Cho, S. J.; Kim, K., Hydrolytic Transformation of Microporous Metal–Organic Frameworks to Hierarchical Micro- and Mesoporous MOFs. *Angew. Chem. Int. Ed.* **2015,** *54* (45), 13273-13278.
68. Feng, L.; Yuan, S.; Zhang, L.-L.; Tan, K.; Li, J.-L.; Kirchon, A.; Liu, L.-M.; Zhang, P.; Han, Y.; Chabal, Y. J.; Zhou, H.-C., Creating Hierarchical Pores by Controlled Linker Thermolysis in Multivariate Metal–Organic Frameworks. *J. Am. Chem. Soc.* **2018,** *140* (6), 2363-2372.
69. Guillerm, V.; Xu, H.; Albalad, J.; Imaz, I.; Maspoch, D., Postsynthetic Selective Ligand Cleavage by Solid–Gas Phase Ozonolysis Fuses Micropores into Mesopores in Metal–Organic Frameworks. *J. Am. Chem. Soc.* **2018,** *140* (44), 15022-15030.
70. Horike, S.; Dincă, M.; Tamaki, K.; Long, J. R., Size-Selective Lewis Acid Catalysis in a Microporous Metal-Organic Framework with Exposed Mn2+ Coordination Sites. *J. Am. Chem. Soc.* **2008,** *130* (18), 5854-5855.
71. Vermoortele, F.; Vandichel, M.; Van de Voorde, B.; Ameloot, R.; Waroquier, M.; Van Speybroeck, V.; De Vos, D. E., Electronic Effects of Linker Substitution on Lewis Acid Catalysis with Metal–Organic Frameworks. *Angew. Chem. Int. Ed.* **2012,** *51* (20), 4887-4890.
72. Mondloch, J. E.; Katz, M. J.; Isley Iii, W. C.; Ghosh, P.; Liao, P.; Bury, W.; Wagner, G. W.; Hall, M. G.; DeCoste, J. B.; Peterson, G. W.; Snurr, R. Q.; Cramer, C. J.; Hupp, J. T.; Farha, O. K., Destruction of chemical warfare agents using metal–organic frameworks. *Nat. Mater.* **2015,** *14* (5), 512-516.
73. Yang, D.; Ortuño, M. A.; Bernales, V.; Cramer, C. J.; Gagliardi, L.; Gates, B. C., Structure and Dynamics of Zr6O8 Metal–Organic Framework Node Surfaces Probed with Ethanol Dehydration as a Catalytic Test Reaction. *J. Am. Chem. Soc.* **2018,** *140* (10), 3751-3759.
74. Ji, P.; Feng, X.; Oliveres, P.; Li, Z.; Murakami, A.; Wang, C.; Lin, W., Strongly Lewis Acidic Metal–Organic Frameworks for Continuous Flow Catalysis. *J. Am. Chem. Soc.* **2019,** *141* (37), 14878-14888.
75. Copéret, C., Surface and Interfacial Chemistry. *CHIMIA International Journal for Chemistry* **2012,** *66* (3), 125-129.
76. Feng, X.; Ji, P.; Li, Z.; Drake, T.; Oliveres, P.; Chen, E. Y.; Song, Y.; Wang, C.; Lin, W., Aluminum Hydroxide Secondary Building Units in a Metal–Organic Framework Support Earth-Abundant Metal Catalysts for Broad-Scope Organic Transformations. *ACS Catal.* **2019,** *9* (4), 3327-3337.
77. Ji, P.; Drake, T.; Murakami, A.; Oliveres, P.; Skone, J. H.; Lin, W., Tuning Lewis Acidity of Metal–Organic Frameworks via Perfluorination of Bridging Ligands: Spectroscopic, Theoretical, and Catalytic Studies. *J. Am. Chem. Soc.* **2018,** *140* (33), 10553-10561.
78. Sobańska, K.; Krasowska, A.; Mazur, T.; Podolska-Serafin, K.; Pietrzyk, P.; Sojka, Z., Diagnostic Features of EPR Spectra of Superoxide Intermediates on Catalytic Surfaces and Molecular Interpretation of Their g and A Tensors. *Top. Catal.* **2015,** *58* (12), 796-810.
79. Ohkubo, K.; Menon, S. C.; Orita, A.; Otera, J.; Fukuzumi, S., Quantitative Evaluation of Lewis Acidity of Metal Ions with Different Ligands and Counterions in Relation to the Promoting Effects of Lewis Acids on Electron Transfer Reduction of Oxygen. *J. Org. Chem.* **2003,** *68* (12), 4720-4726.
80. Jack, L.; Yellowlees, L. J.; Parsons, S., CCDC 660772: Experimental Crystal Structure Determination. Cambridge Crystallographic Data Centre: 2008.
81. Serrano-Ruiz, J. C.; Dumesic, J. A., Catalytic routes for the conversion of biomass into liquid hydrocarbon transportation fuels. *Energy Environ. Sci.* **2011,** *4* (1), 83-99.
82. García, V.; Päkkilä, J.; Ojamo, H.; Muurinen, E.; Keiski, R. L., Challenges in biobutanol production: How to improve the efficiency? *Renew. Sustain. Energy Rev.* **2011,** *15* (2), 964-980.
83. Gallezot, P., Conversion of biomass to selected chemical products. *Chem. Soc. Rev.* **2012,** *41* (4), 1538-1558.

84. Ruppert, A. M.; Weinberg, K.; Palkovits, R., Hydrogenolysis Goes Bio: From Carbohydrates and Sugar Alcohols to Platform Chemicals. *Angew. Chem. Int. Ed.* **2012,** *51* (11), 2564-2601.
85. McLaughlin, M. P.; Adduci, L. L.; Becker, J. J.; Gagné, M. R., Iridium-Catalyzed Hydrosilylative Reduction of Glucose to Hexane(s). *J. Am. Chem. Soc.* **2013,** *135* (4), 1225-1227.
86. Yu, X.; Seo, S.; Marks, T. J., Effective, Selective Hydroalkoxylation/Cyclization of Alkynyl and Allenyl Alcohols Mediated by Lanthanide Catalysts. *J. Am. Chem. Soc.* **2007,** *129* (23), 7244-7245.
87. Dzudza, A.; Marks, T. J., Efficient Intramolecular Hydroalkoxylation/Cyclization of Unactivated Alkenols Mediated by Lanthanide Triflate Ionic Liquids. *Org. Lett.* **2009,** *11* (7), 1523-1526.
88. Dzudza, A.; Marks, T. J., Efficient Intramolecular Hydroalkoxylation of Unactivated Alkenols Mediated by Recyclable Lanthanide Triflate Ionic Liquids: Scope and Mechanism. *Chem.: Eur. J* **2010,** *16* (11), 3403-3422.
89. Lohr, T. L.; Marks, T. J., Orthogonal tandem catalysis. *Nat. Chem.* **2015,** *7* (6), 477-482.
90. Zhao, C.; Kou, Y.; Lemonidou, A. A.; Li, X.; Lercher, J. A., Highly Selective Catalytic Conversion of Phenolic Bio-Oil to Alkanes. *Angew. Chem. Int. Ed.* **2009,** *48* (22), 3987-3990.
91. Geboers, J.; Van de Vyver, S.; Carpentier, K.; de Blochouse, K.; Jacobs, P.; Sels, B., Efficient catalytic conversion of concentrated cellulose feeds to hexitols with heteropoly acids and Ru on carbon. *Chem. Commun.* **2010,** *46* (20), 3577-3579.
92. Yan, N.; Yuan, Y.; Dykeman, R.; Kou, Y.; Dyson, P. J., Hydrodeoxygenation of Lignin-Derived Phenols into Alkanes by Using Nanoparticle Catalysts Combined with Brønsted Acidic Ionic Liquids. *Angew. Chem. Int. Ed.* **2010,** *49* (32), 5549-5553.
93. Geboers, J.; Van de Vyver, S.; Carpentier, K.; Jacobs, P.; Sels, B., Hydrolytic hydrogenation of cellulose with hydrotreated caesium salts of heteropoly acids and Ru/C. *Green Chem.* **2011,** *13* (8), 2167-2174.
94. Alonso, D. M.; Wettstein, S. G.; Dumesic, J. A., Bimetallic catalysts for upgrading of biomass to fuels and chemicals. *Chem. Soc. Rev.* **2012,** *41* (24), 8075-8098.
95. Olson, E. S.; Aulich, T. R.; Sharma, R. K.; Timpe, R. C., Ester fuels and chemicals from biomass. *Appl. Biochem. Biotechnol.* **2003,** *108* (1), 843-851.
96. Shahid, E. M.; Jamal, Y., Production of biodiesel: A technical review. *Renew. Sustain. Energy Rev.* **2011,** *15* (9), 4732-4745.
97. Borugadda, V. B.; Goud, V. V., Biodiesel production from renewable feedstocks: Status and opportunities. *Renew. Sustain. Energy Rev.* **2012,** *16* (7), 4763-4784.
98. Lestari , S.; Mäki-Arvela, P.; Beltramini, J.; Lu, G. Q. M.; Murzin, D. Y., Transforming Triglycerides and Fatty Acids into Biofuels. *ChemSusChem* **2009,** *2* (12), 1109-1119.
99. Choudhary, T. V.; Phillips, C. B., Renewable fuels via catalytic hydrodeoxygenation. *Appl. Catal., A* **2011,** *397* (1), 1-12.
100. Zhao, C.; Brück, T.; Lercher, J. A., Catalytic deoxygenation of microalgae oil to green hydrocarbons. *Green Chem.* **2013,** *15* (7), 1720-1739.
101. Gosselink, R. W.; Hollak, S. A. W.; Chang, S.-W.; van Haveren, J.; de Jong, K. P.; Bitter, J. H.; van Es, D. S., Reaction Pathways for the Deoxygenation of Vegetable Oils and Related Model Compounds. *ChemSusChem* **2013,** *6* (9), 1576-1594.
102. Lohr, T. L.; Li, Z.; Assary, R. S.; Curtiss, L. A.; Marks, T. J., Mono- and tri-ester hydrogenolysis using tandem catalysis. Scope and mechanism. *Energy Environ. Sci.* **2016,** *9* (2), 550-564.

TOC:

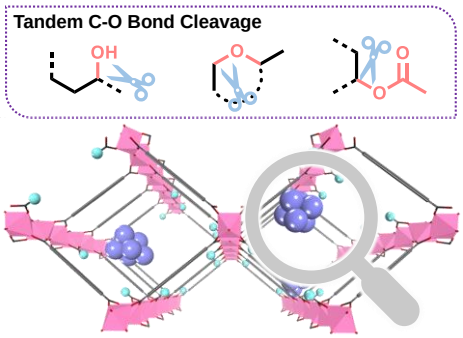

Synergistic **Lewis acidic** and **metallic Pd** sites in a MOF